# Electronic Supplementary Information (ESI)

## *In situ* semi-transformation from heterometallic MOFs to Fe-Ni LDH/MOF hierarchical architectures for boosted oxygen evolution reaction

Jiamin Huo, [a] Ying Wang,*[a] Liting Yan, [b] Yingying Xue, [a] Shuni Li, [a] Mancheng Hu,*[a] Yucheng Jiang, [a] and Quan-Guo Zhai*[a]

[a] Key Laboratory of Macromolecular Science of Shaanxi Province, Key Laboratory of Applied Surface and Colloid Chemistry, Ministry of Education, School of Chemistry & chemical Engineering, Shaanxi Normal University, Xi'an, Shaanxi, 710062, China

[b] School of Materials Science and Engineering, Qilu University of Technology (Shandong Academy of Sciences), No.3501, Daxue Road, Changqing District, Jinan, 250353, China

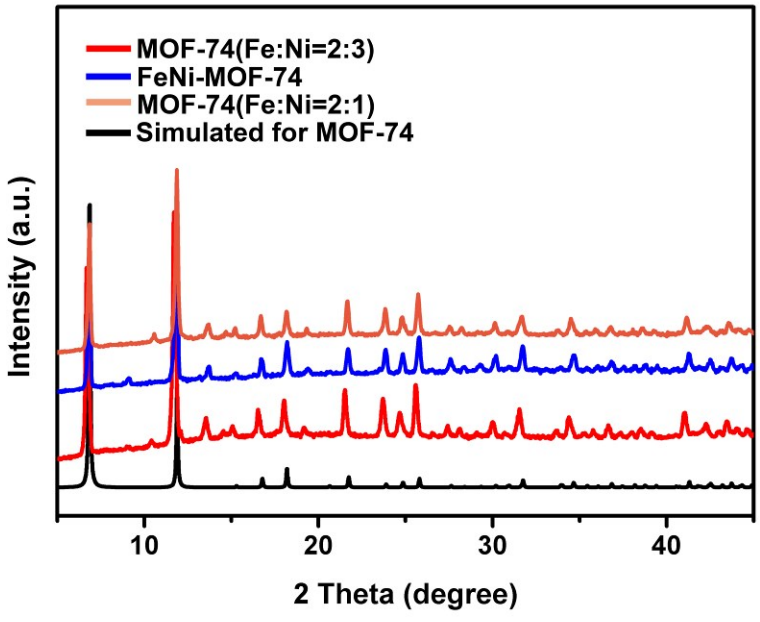


**Fig. S1** PXRD patterns of FeNi-MOF-74 precursors with different metal radio.

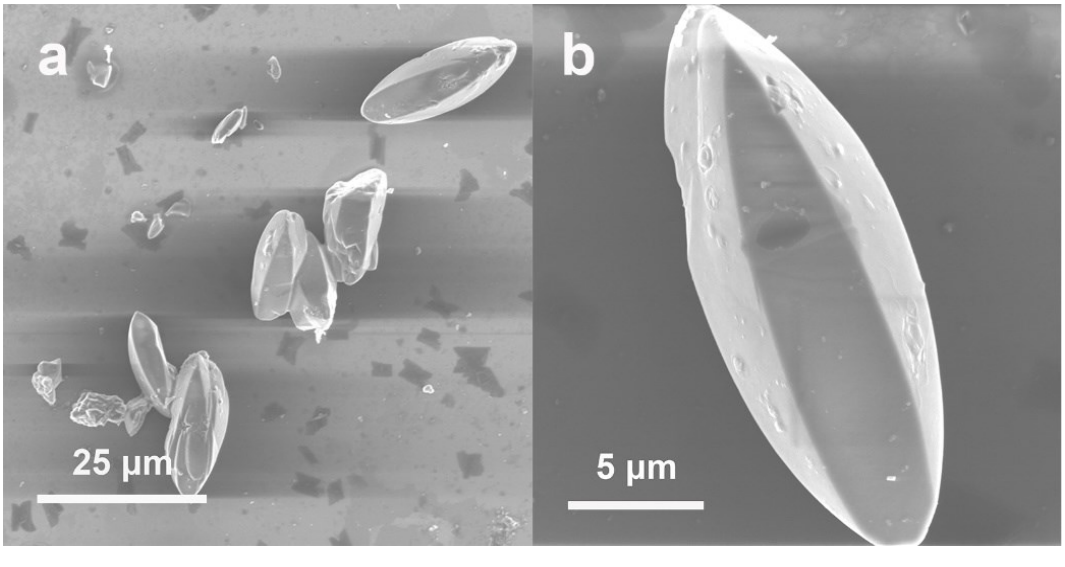


**Fig. S2** The SEM of MOF-74(Fe:Ni=2:1).

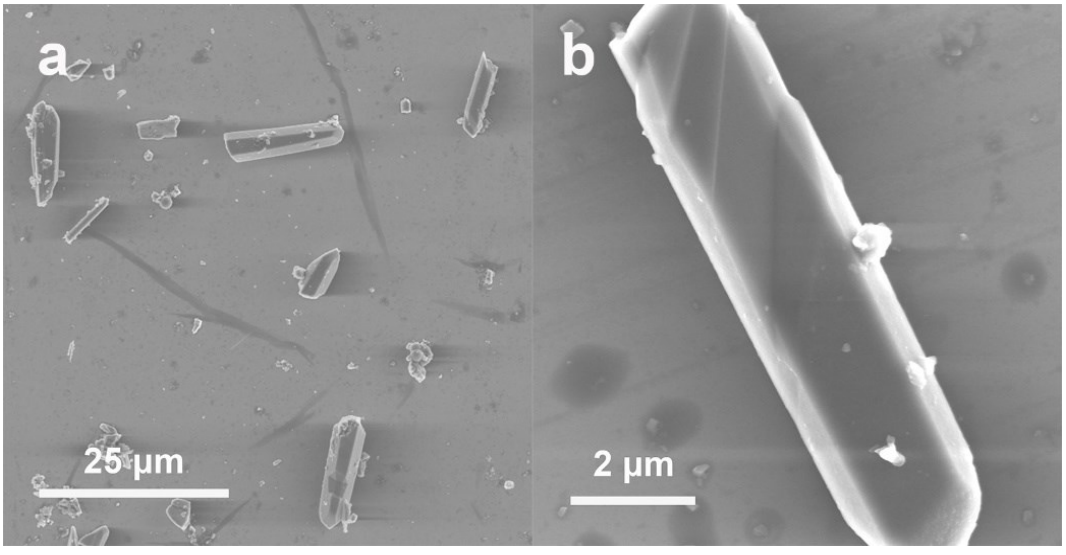


**Fig. S3** The SEM of FeNi-MOF-74 (Fe:Ni=1:1).

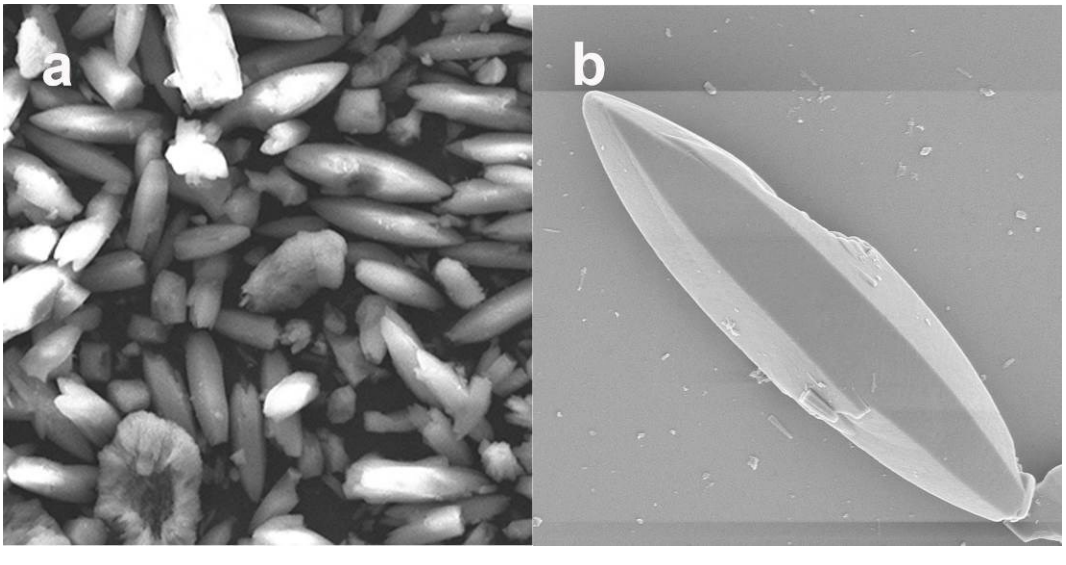


**Fig. S4** The SEM of MOF-74 (Fe:Ni=2:3).

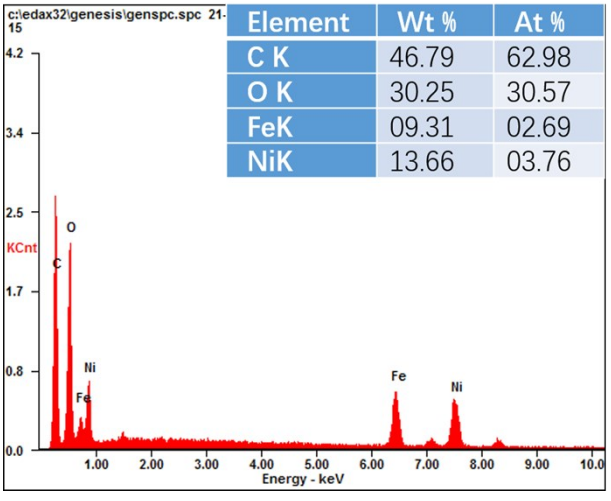


| Element | Wt % | At % |
|---|---|---|
| C K | 46.79 | 62.98 |
| O K | 30.25 | 30.57 |
| FeK | 09.31 | 02.69 |
| NiK | 13.66 | 03.76 |

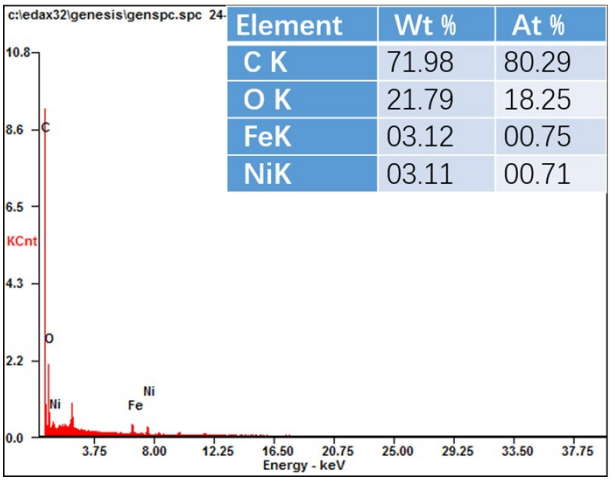


| Element | Wt % | At % |
|---|---|---|
| C K | 71.98 | 80.29 |
| O K | 21.79 | 18.25 |
| FeK | 03.12 | 00.75 |
| NiK | 03.11 | 00.71 |

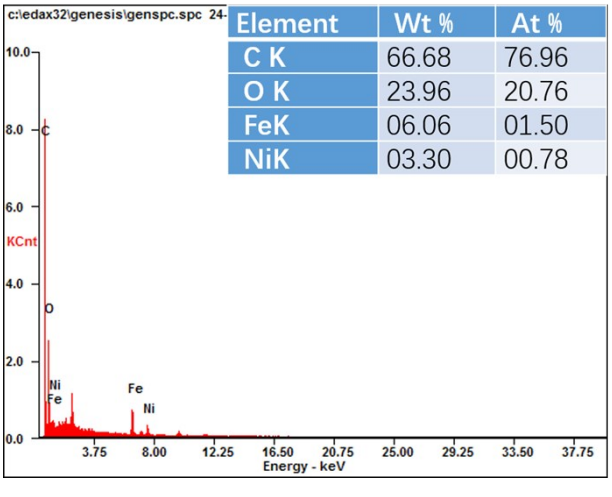


| Element | Wt % | At % |
|---|---|---|
| C K | 66.68 | 76.96 |
| O K | 23.96 | 20.76 |
| FeK | 06.06 | 01.50 |
| NiK | 03.30 | 00.78 |

**Fig. S5** EDS of MOF-74(Fe:Ni=2:3), FeNi-MOF-74 and MOF-74(Fe:Ni=2:1).

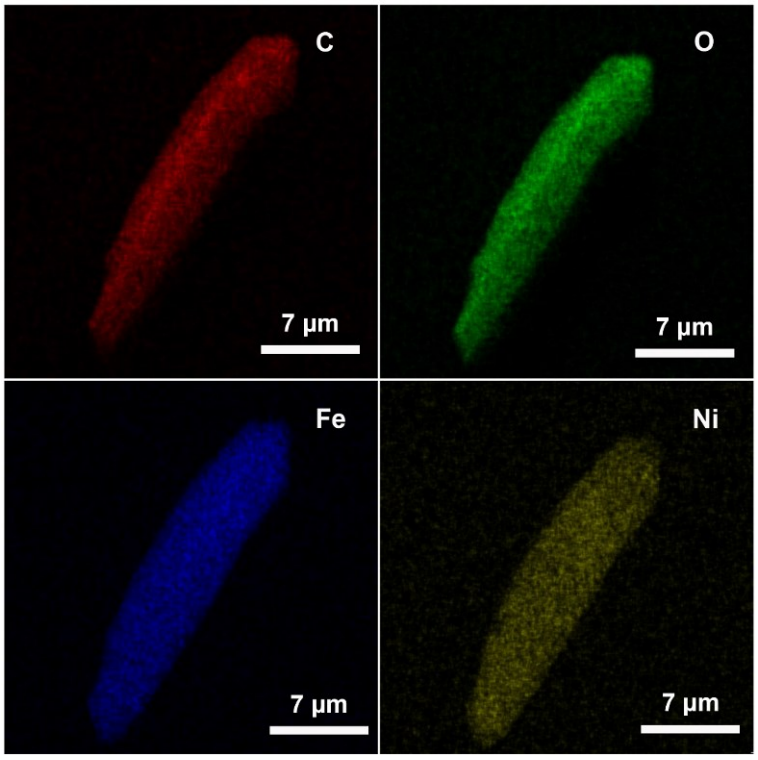


**Fig. S6** Elemental mapping images of C, O, Fe, and Ni in FeNi-MOF-74.

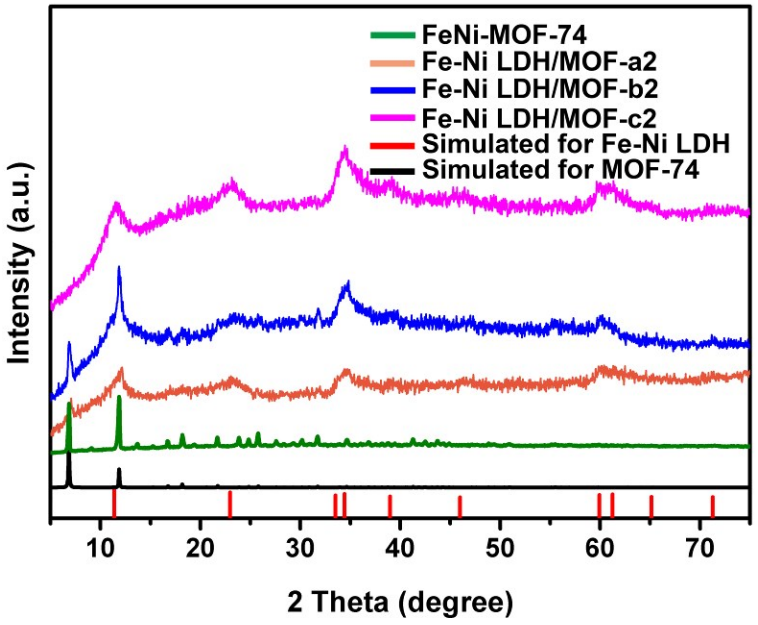


**Fig. S7** PXRD patterns of Fe-Ni LDH/MOF-a2, Fe-Ni LDH/MOF-b2, Fe-Ni LDH/MOF-c2 and FeNi-MOF-74 using FeNi-MOF-74 (Fe:Ni=1:1) as precursor.

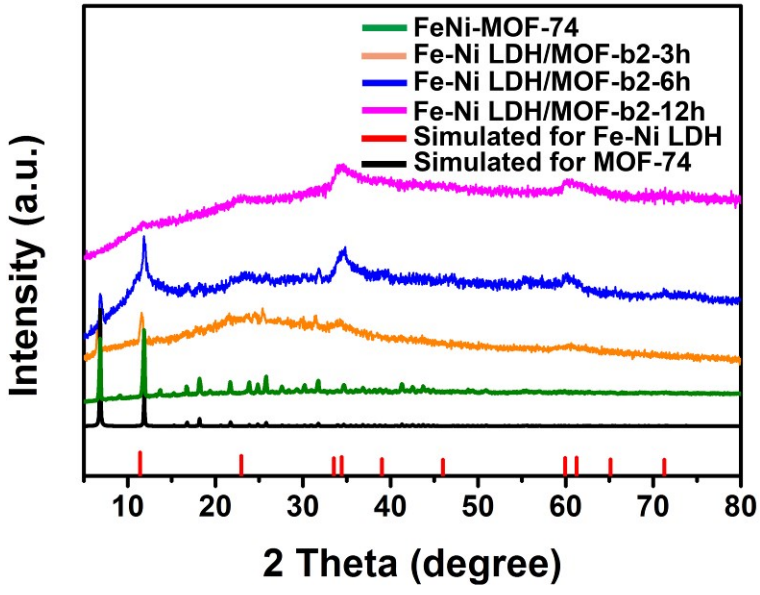


**Fig. S8** PXRD patterns of Fe-Ni LDH/MOF-b2-3h, Fe-Ni LDH/MOF-b2-6h, Fe-Ni LDH/MOF-b2-12h and FeNi-MOF-74 using FeNi-MOF-74 (Fe:Ni=1:1) as precursor.

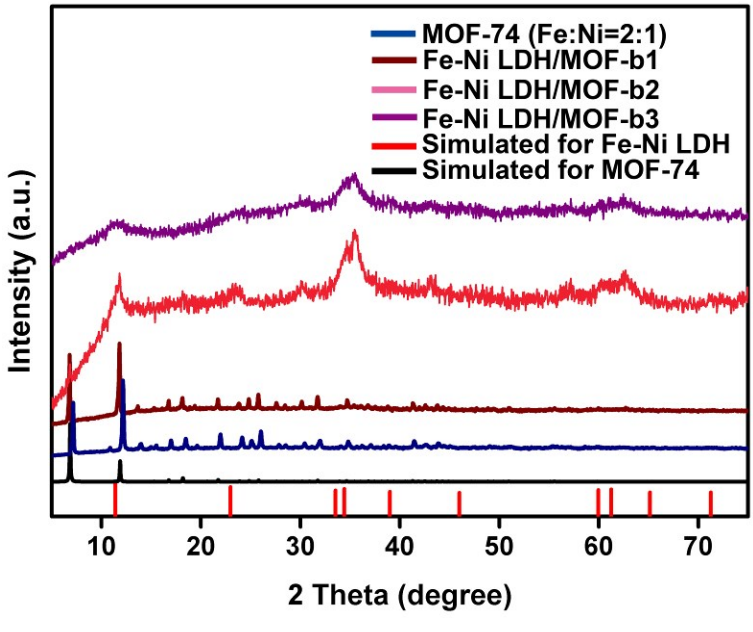


**Fig. S9** PXRD patterns of Fe-Ni LDH/MOF-b1, Fe-Ni LDH/MOF-b2, Fe-Ni LDH/MOF-b3 and MOF-74(Fe:Ni=2:1) using FeNi-MOF-74(Fe:Ni=2:1) as precursor.

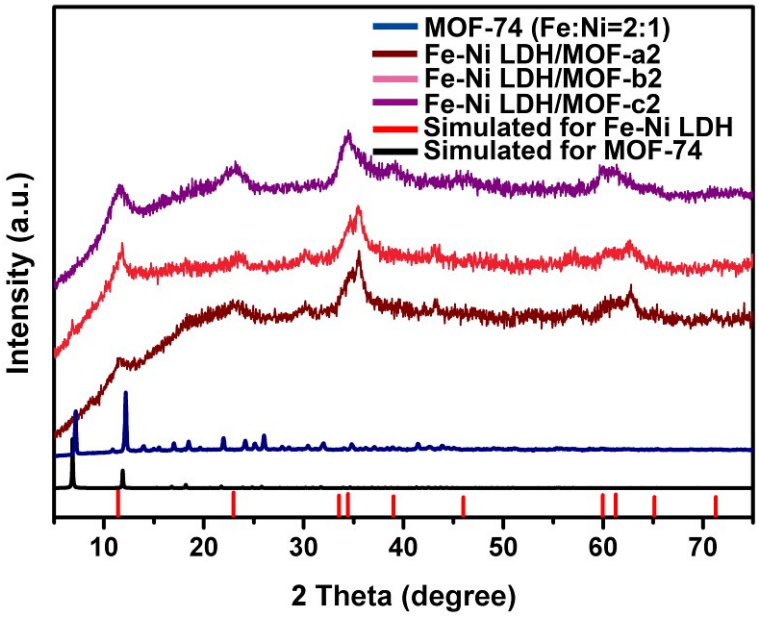


**Fig. S10** PXRD patterns of Fe-Ni LDH/MOF-a2, Fe-Ni LDH/MOF-b2, Fe-Ni LDH/MOF-c2 and MOF-74(Fe:Ni=2:1) using MOF-74(Fe:Ni=2:1) as precursor.

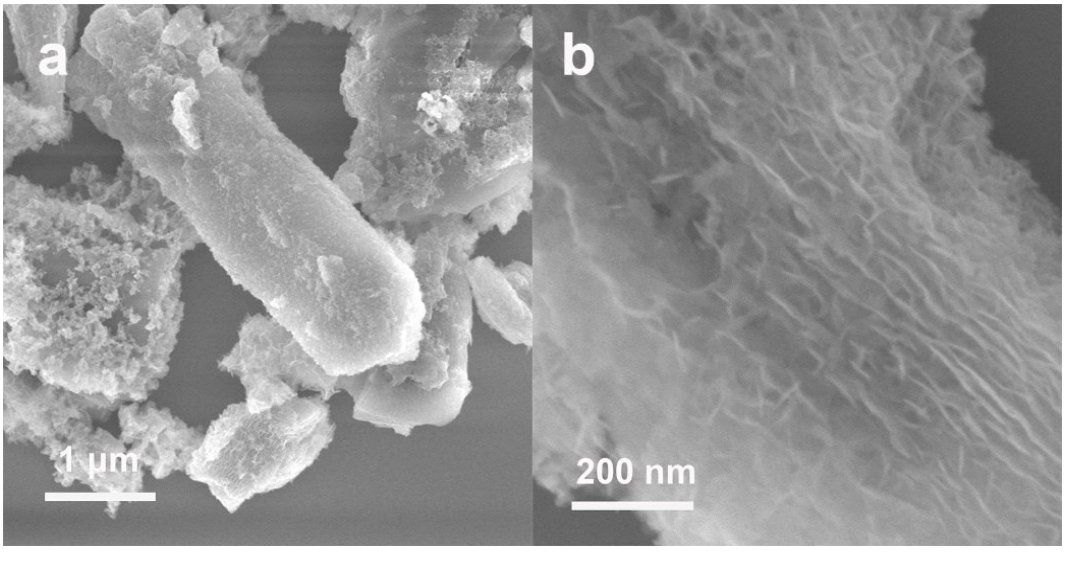


**Fig. S11** The SEM of Fe-Ni LDH/MOF-b1 using FeNi-MOF-74 as a precursor.

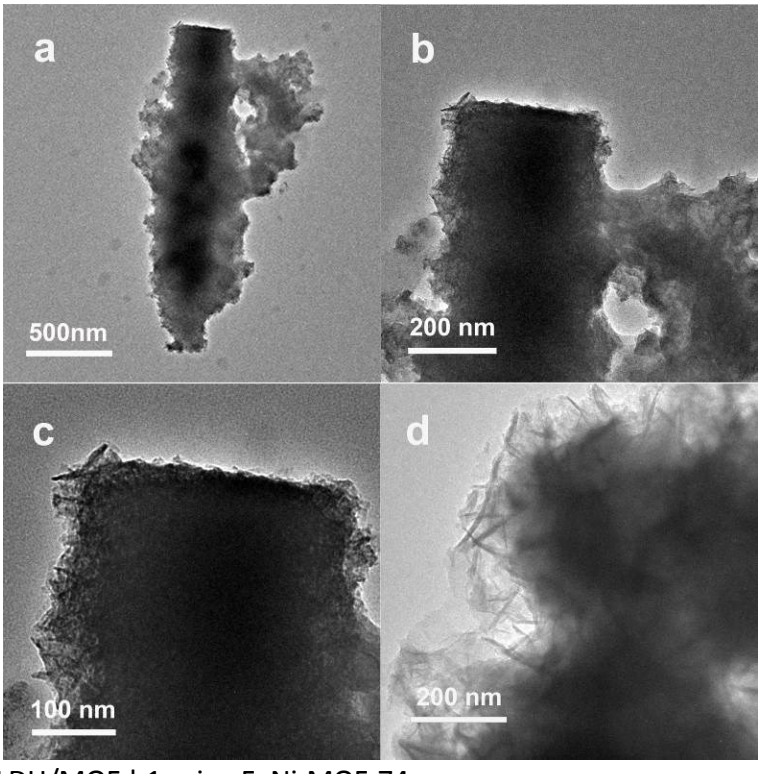


**Fig. S12** The TEM of Fe-Ni LDH/MOF-b1 using FeNi-MOF-74 as a precursor.

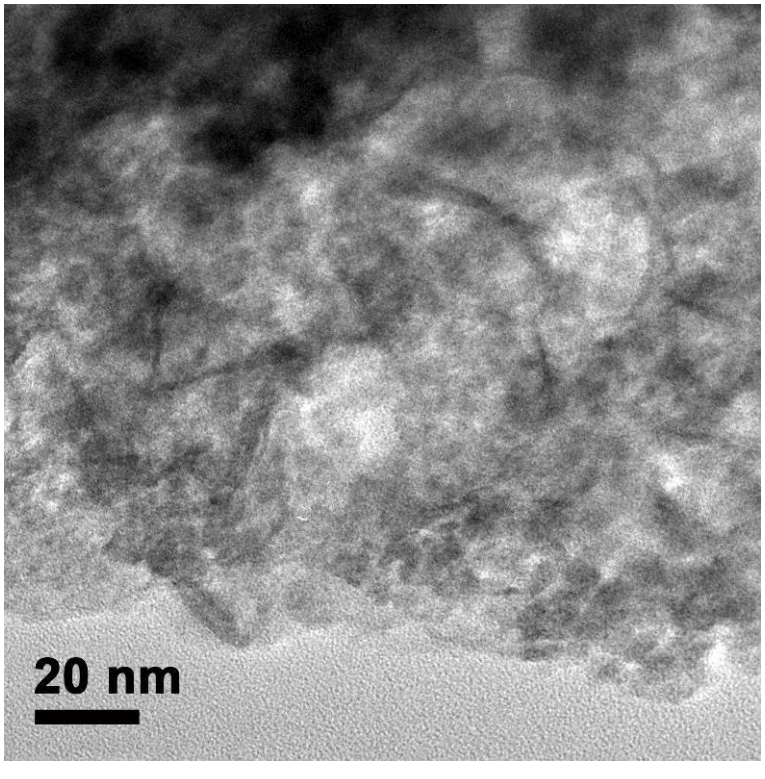


**Fig. S13** TEM image of ultra-thin LDH nanoarrays near the edge Fe-Ni LDH/MOF-b2**.**

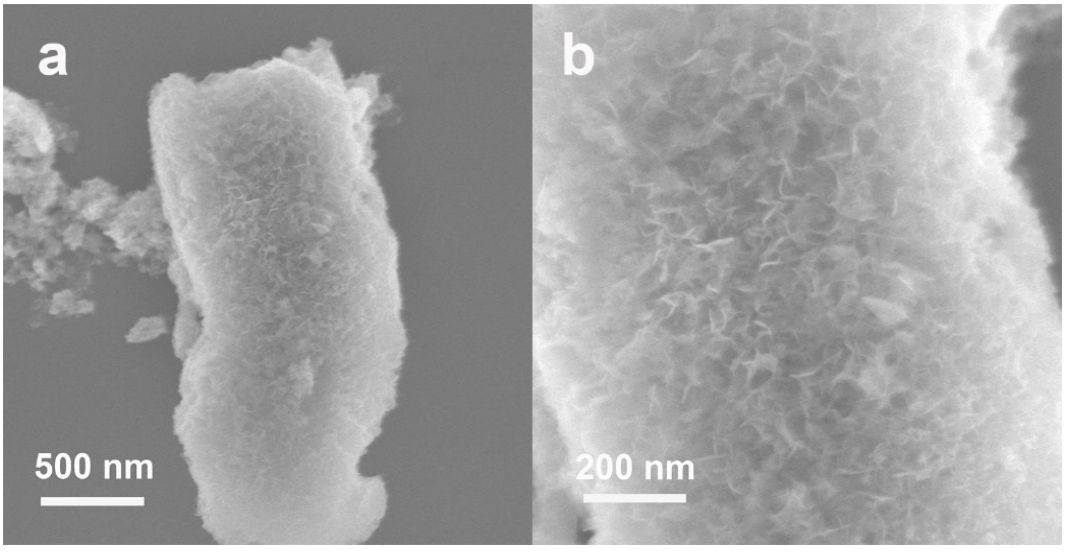


**Fig. S14** The SEM of Fe-Ni LDH/MOF-b3 using FeNi-MOF-74 as a precursor.

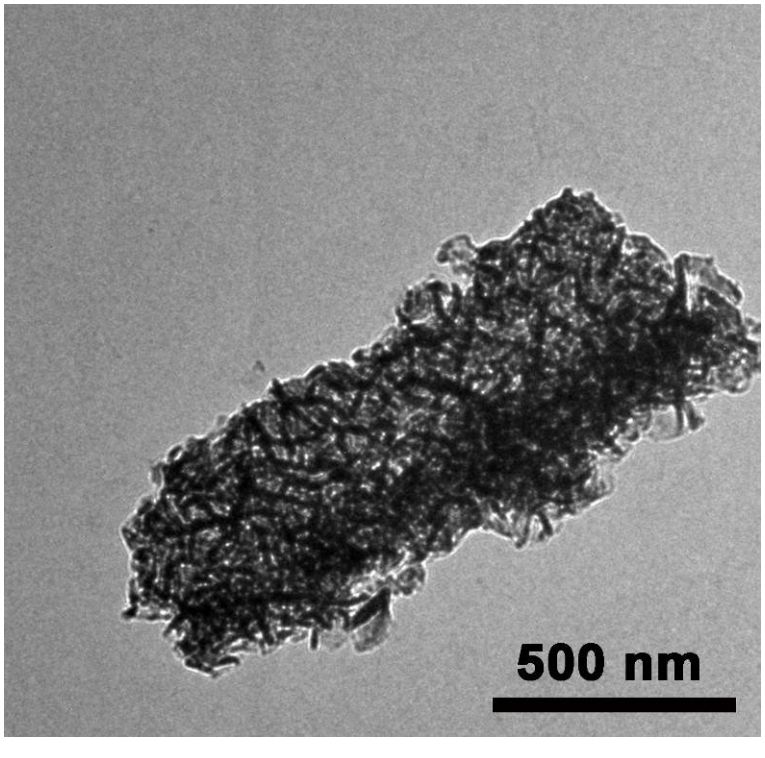


**Fig. S15** The TEM of Fe-Ni LDH/MOF-b3 using FeNi-MOF-74 as a precursor.

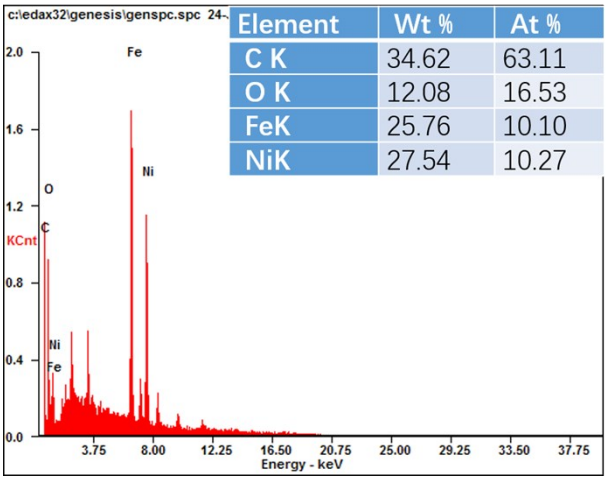


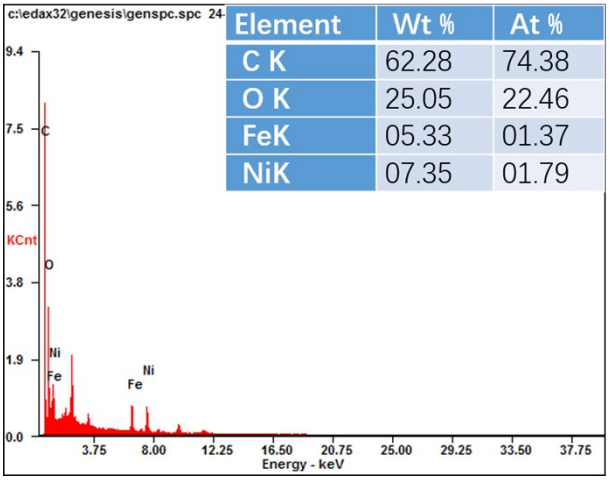


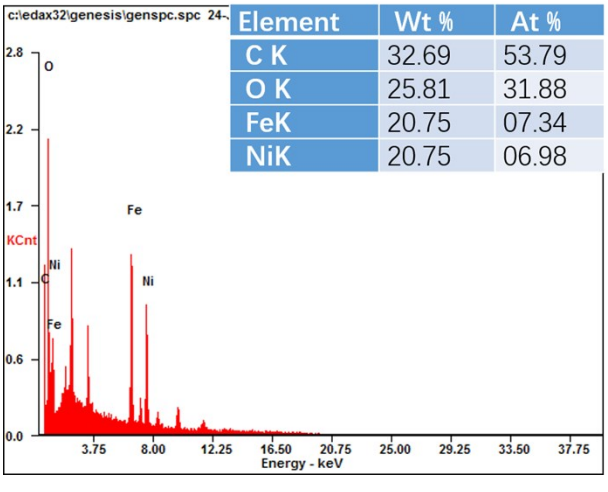


**Fig. S16** EDS of Fe-Ni LDH/MOF-b1, Fe-Ni LDH/MOF-b2 and Fe-Ni LDH/MOF-b3.

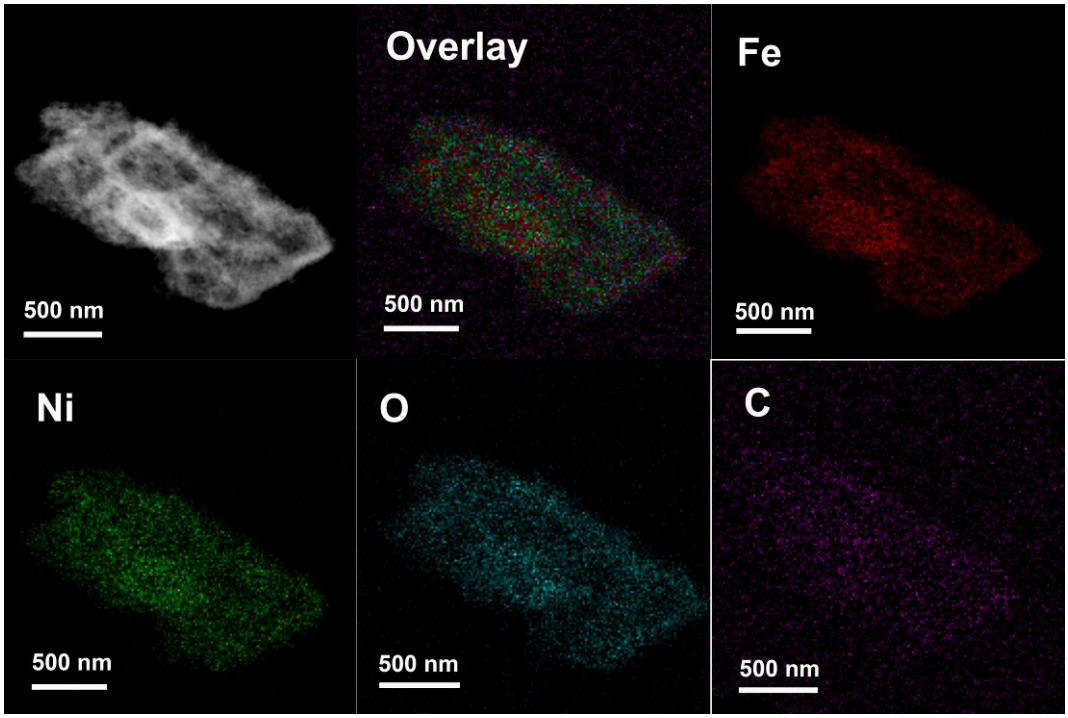


**Fig. S17** Elemental mapping of Fe, Ni, C and O of Fe-Ni LDH/MOF-b2 that by using the FETEM-EDS.

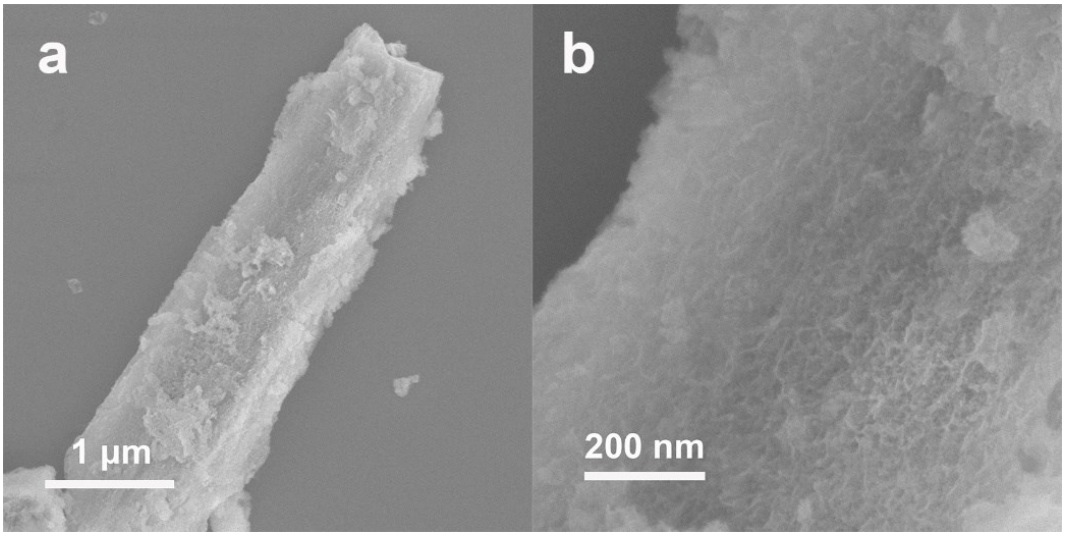


**Fig. S18** The SEM of Fe-Ni LDH/MOF-a2 using FeNi-MOF-74 as a precursor.

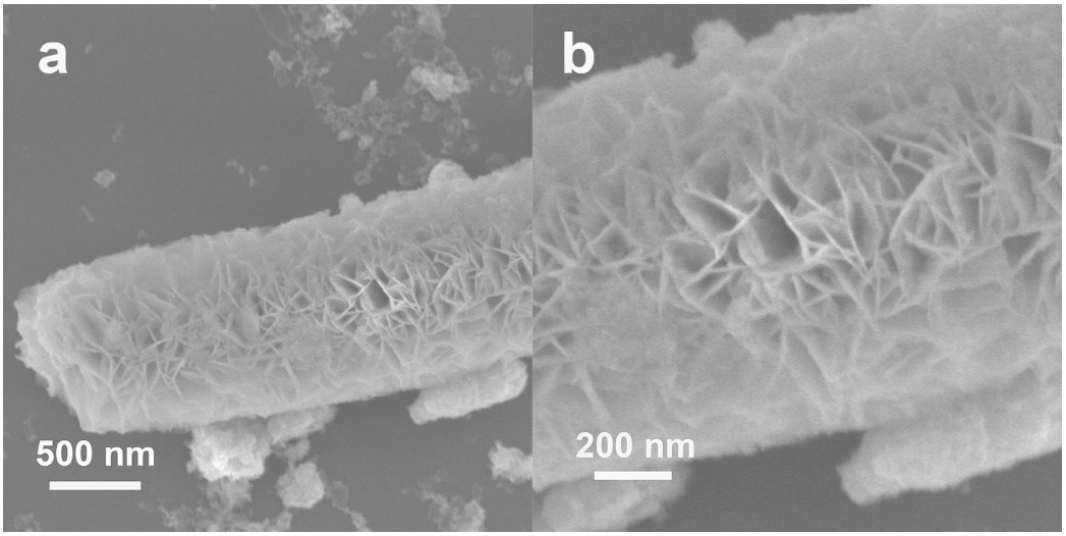


**Fig. S19** The SEM of Fe-Ni LDH/MOF-c2 using FeNi-MOF-74 as a precursor.

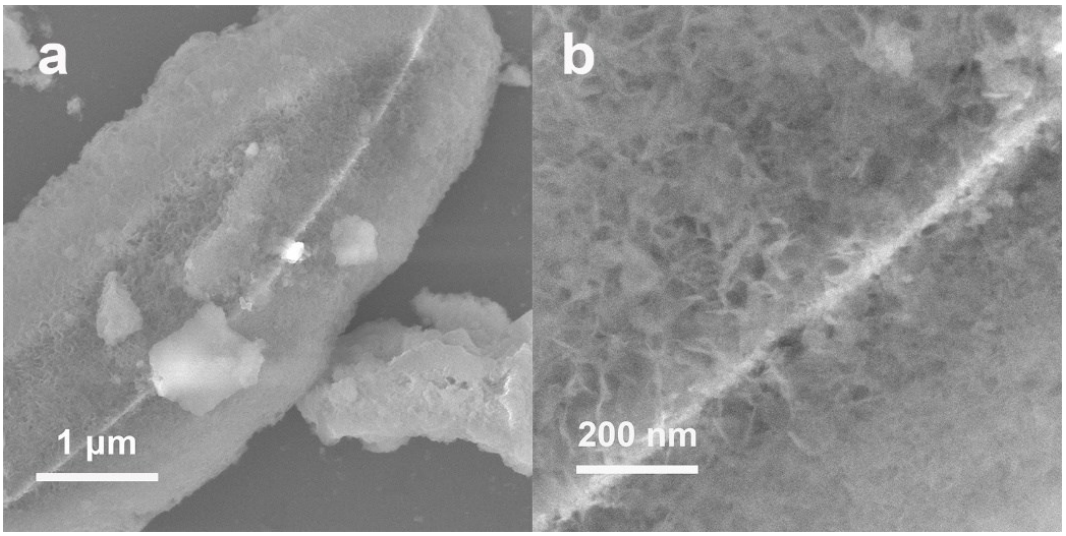


**Fig. S20** The SEM of Fe-Ni LDH/MOF-74 (Fe : Ni = 2 : 1)-b2 using MOF-74(Fe:Ni=2:1) as a precursor.

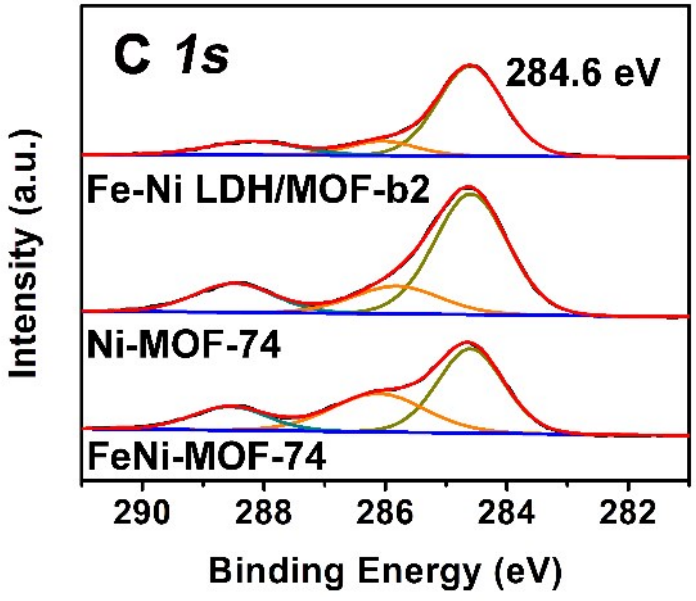


**Fig. S21** The XPS spectra of C *1s* the FeNi-MOF-74, Ni-MOF-74 and Fe-Ni LDH/MOF-b2.

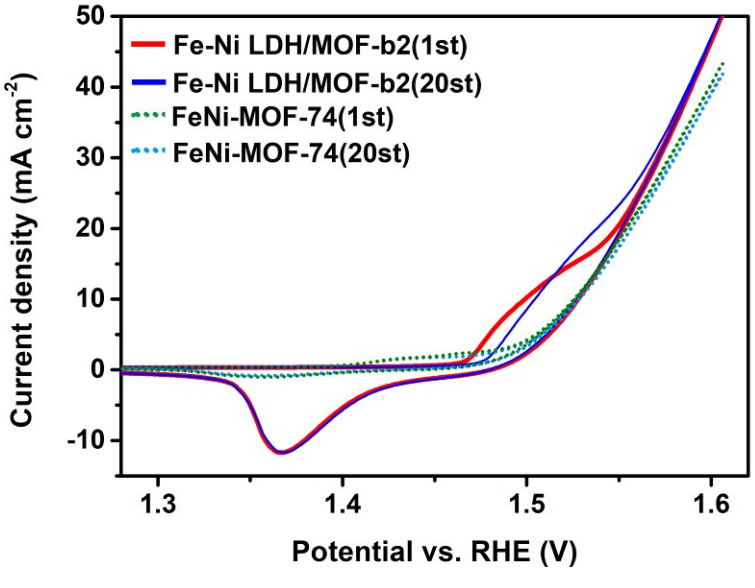


**Fig. S22** The full cyclic voltammograms (CV) of FeNi-MOF-74 and Fe-Ni LDH/MOF-b2 at a scan rate of 10 mV·s$^{-1}$ without *iR* correction.

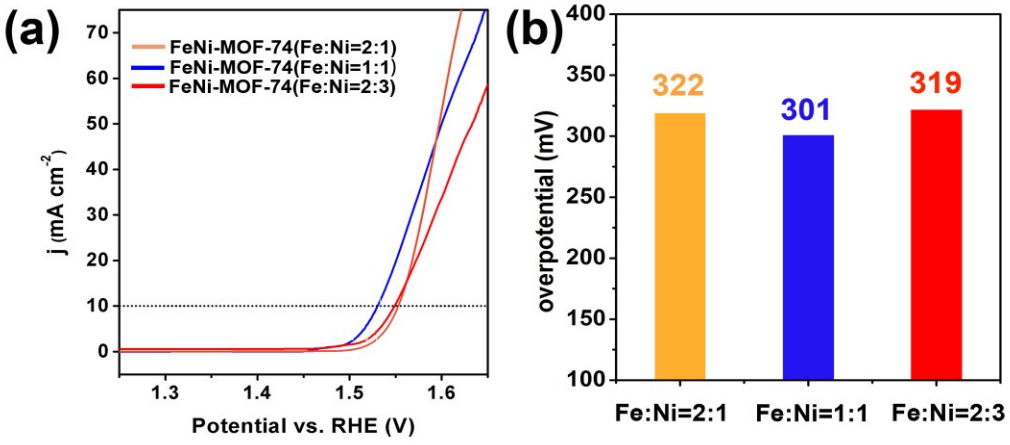


**Fig. S23** (a) The LSV curves of MOF-74(Fe:Ni=2:3), FeNi-MOF-74 and MOF-74(Fe:Ni=2:1); (b) Overpotential at 10 mA·cm$^{-2}$ for different MOF precursors.

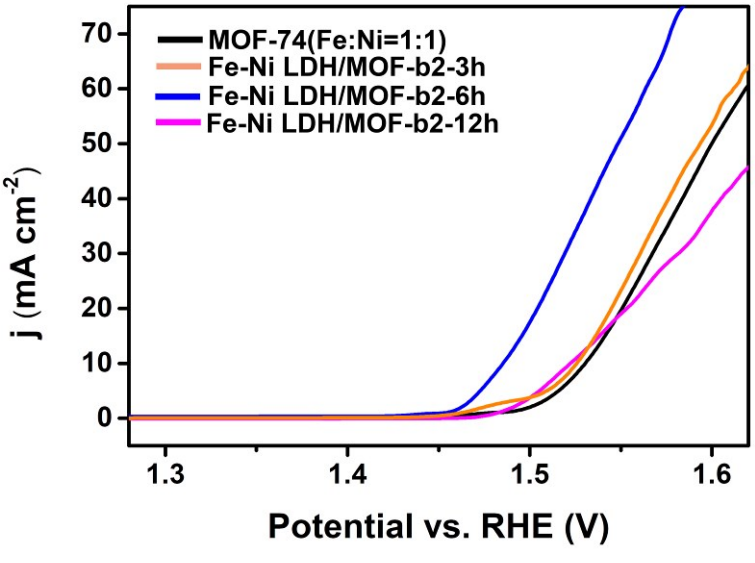


**Fig. S24** The LSV curves of Fe-Ni LDH/MOF-b2-3h, Fe-Ni LDH/MOF-b2-6h, Fe-Ni LDH/MOF-b2-12h and FeNi-MOF-74 using FeNi-MOF-74 as a precursor.

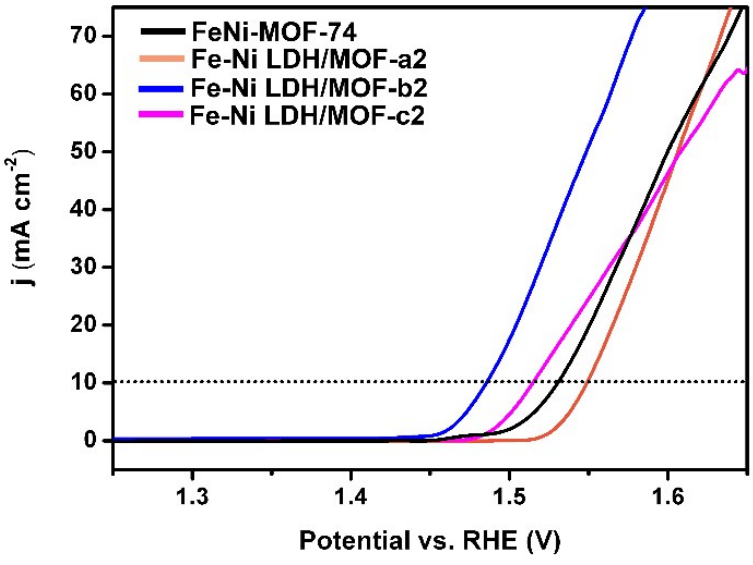


**Fig. S25** The LSV curves of Fe-Ni LDH/MOF-a2, Fe-Ni LDH/MOF-b2, Fe-Ni LDH/MOF-c2 and FeNi-MOF-74 using FeNi-MOF-74 as a precursor.

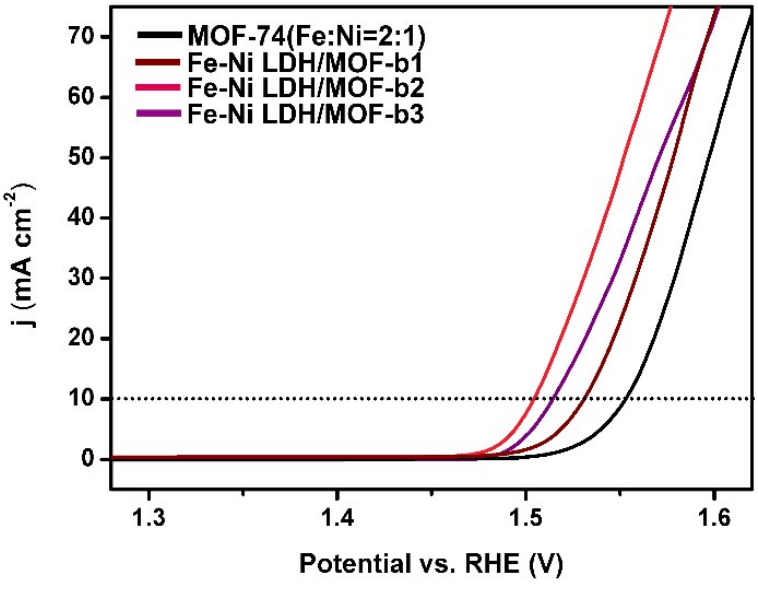


**Fig. S26** The LSV curves of Fe-Ni LDH/MOF-b1, Fe-Ni LDH/MOF-b2, Fe-Ni LDH/MOF-b3 and MOF-74(Fe:Ni=2:1) using MOF-74(Fe:Ni=2:1) as a precursor.

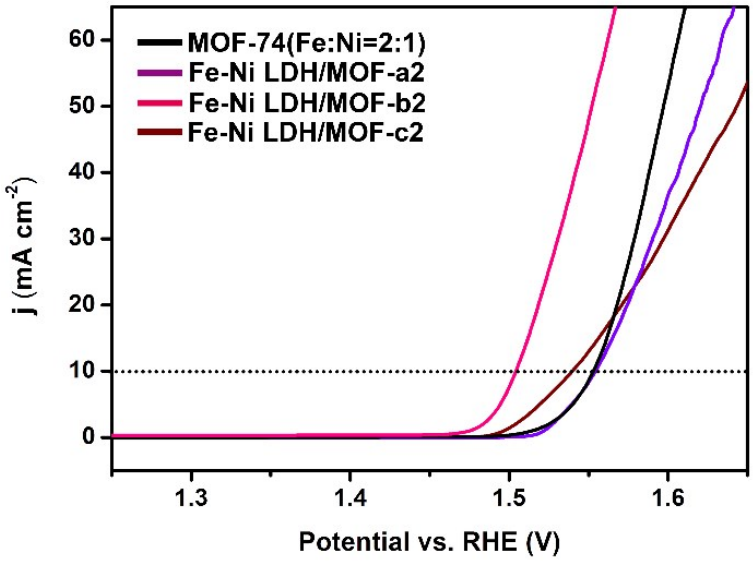


**Fig. S27** The LSV curves of Fe-Ni LDH/MOF-a2, Fe-Ni LDH/MOF-b2, Fe-Ni LDH/MOF-c2 and MOF-74(Fe:Ni=2:1) using MOF-74(Fe:Ni=2:1) as a precursor.

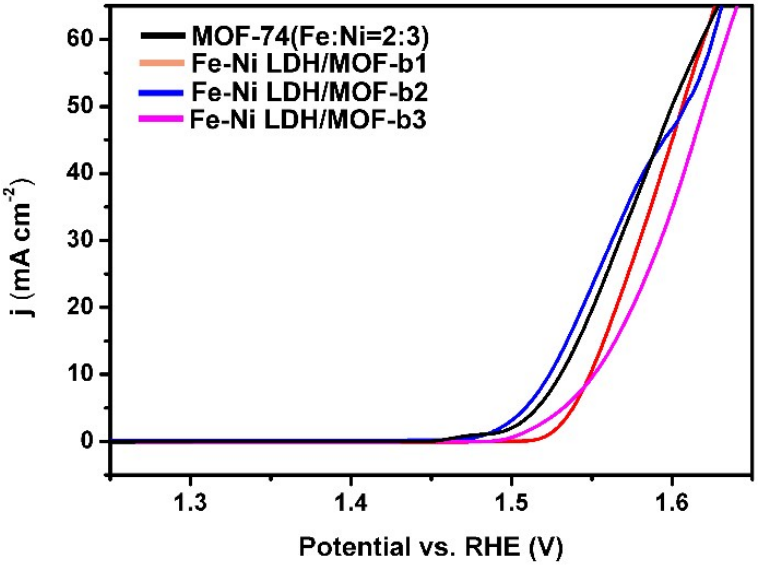


**Fig. S28** The LSV curves of Fe-Ni LDH/MOF-b1, Fe-Ni LDH/MOF-b2, Fe-Ni LDH/MOF-b3 and MOF-74(Fe:Ni=2:3) using MOF-74(Fe:Ni=2:3) as a precursor.

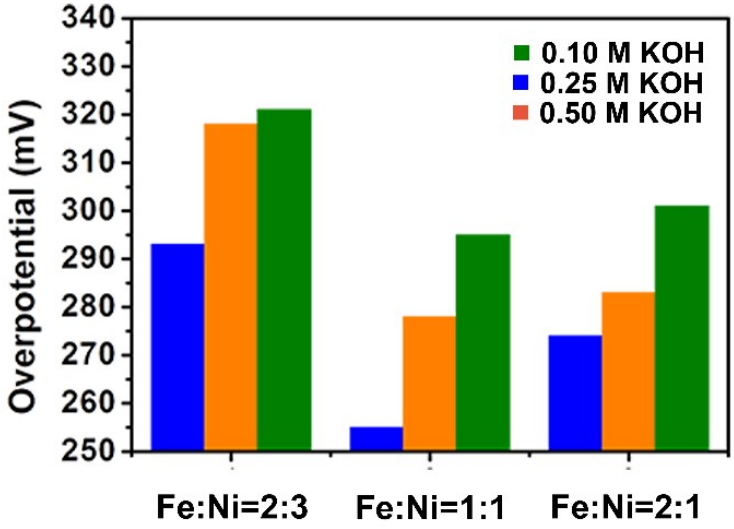


**Fig. S29** Summary of the overpotential from the concentration effect with different MOF precursors.

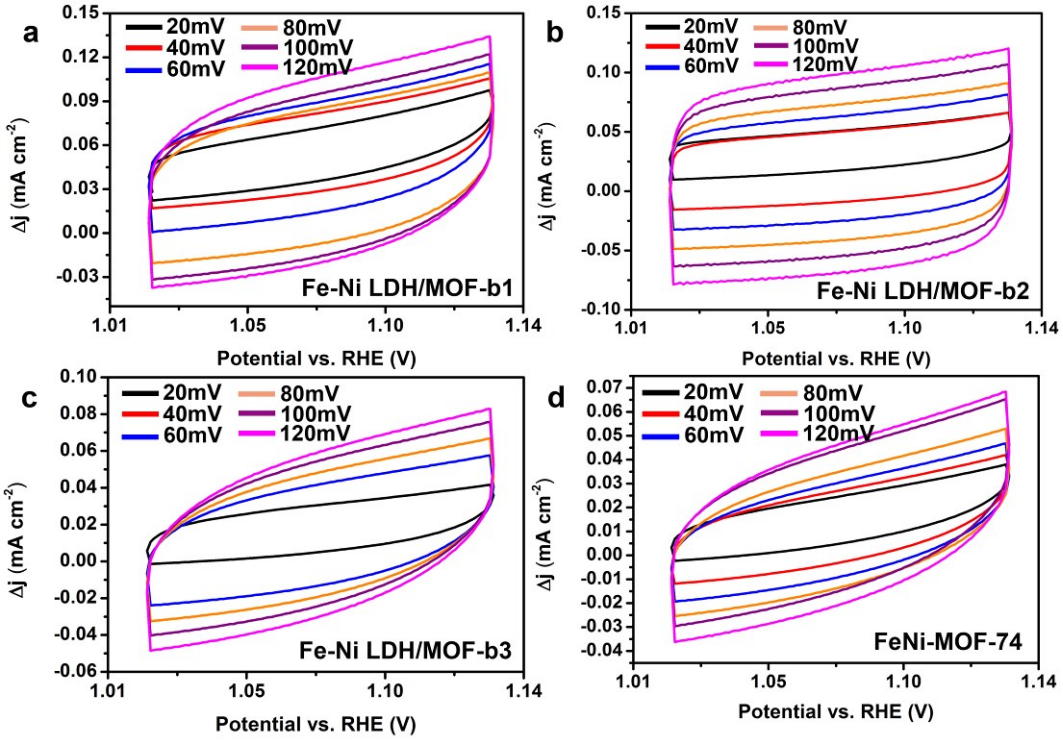


**Fig. S30** The CV curves of the as-prepared Fe-Ni LDH/MOF-b1, Fe-Ni LDH/MOF-b2, Fe-Ni LDH/MOF-b3 and FeNi-MOF-74 at different scan rate of 20, 40, 60, 80, 100 and 120 mV $s^{-1}$.

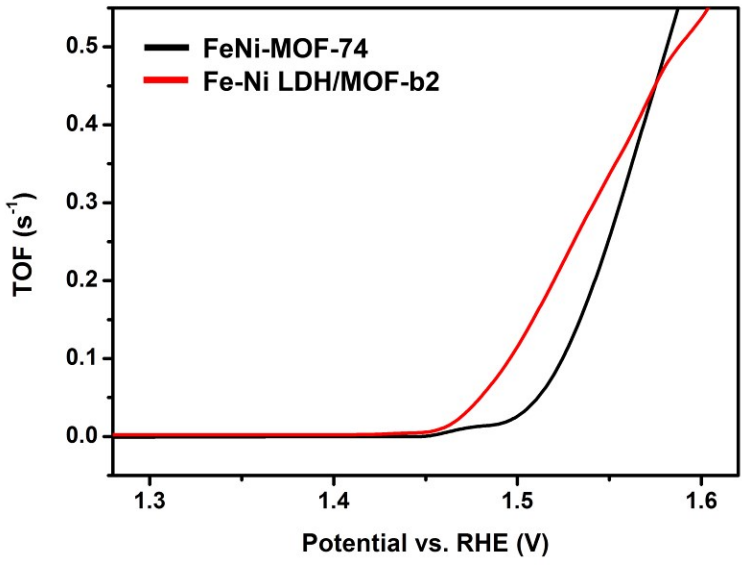


**Fig. S31** TOF curves of FeNi-MOF-74 precursors and the hierarchical Fe-Ni LDH/MOF-b2 for OER reaction at different potentials.

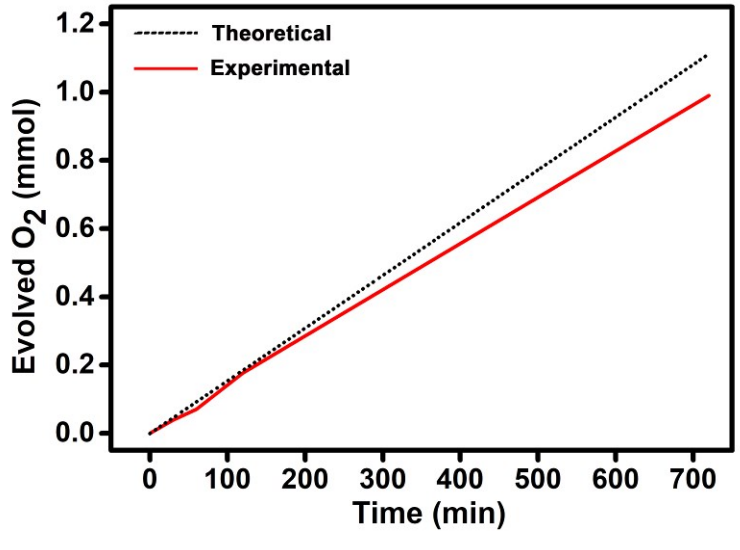


**Fig. S32** Theoretical and experimental amounts of $O_2$ evolved during the OER at the current density of 10 mA·cm$^{-2}$.

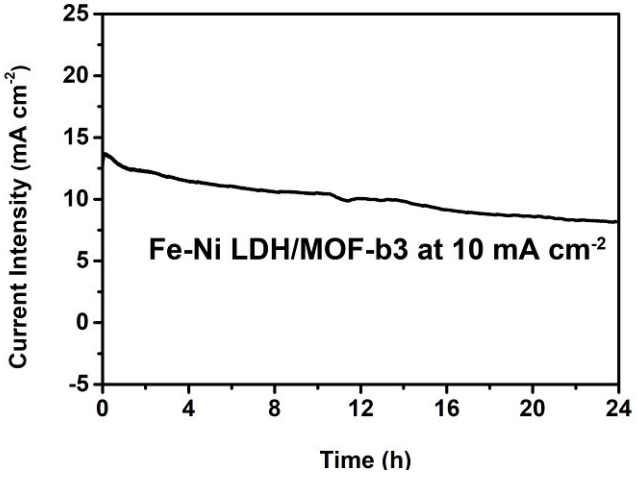


**Fig. S33** Stability test of Fe-Ni LDH/MOF-b3 for 24 h at current density of 10 mA·cm$^{-2}$.

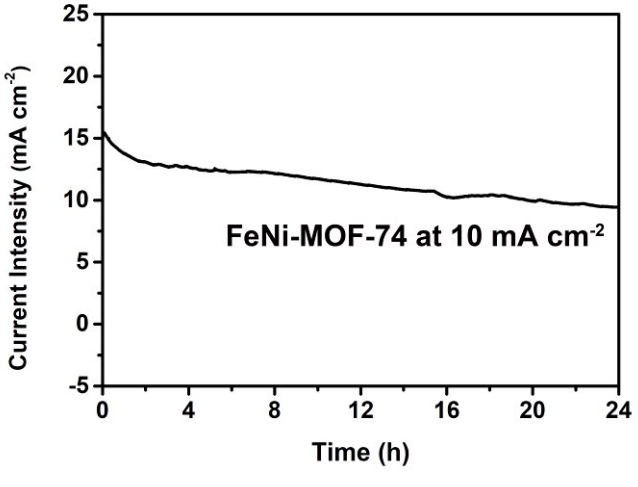


**Fig. S34** Stability test of FeNi-MOF-74 for 24 h at current density of 10 mA·cm$^{-2}$.

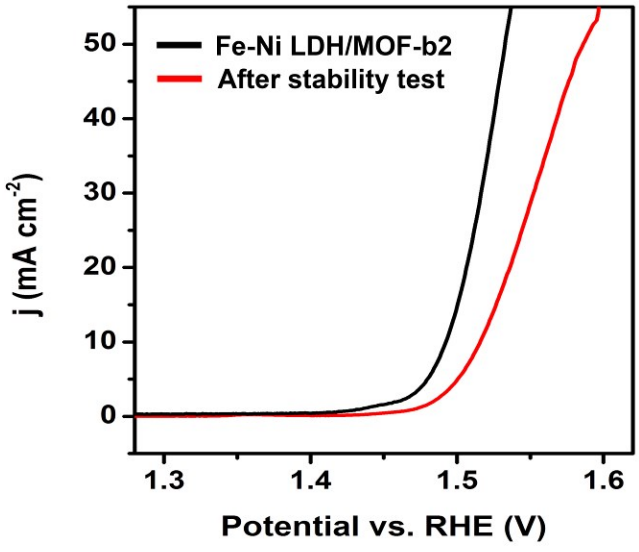


**Fig. S35** LSV curve of Fe-Ni LDH/MOF-b2 after 24h stability testing.

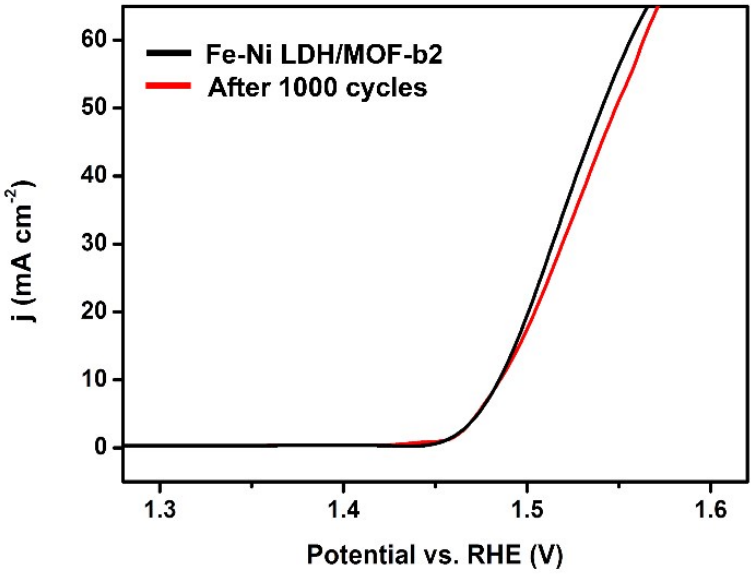


**Fig. S36** The LSV curves of Fe-Ni LDH/MOF-b2 after 1000 cycles.

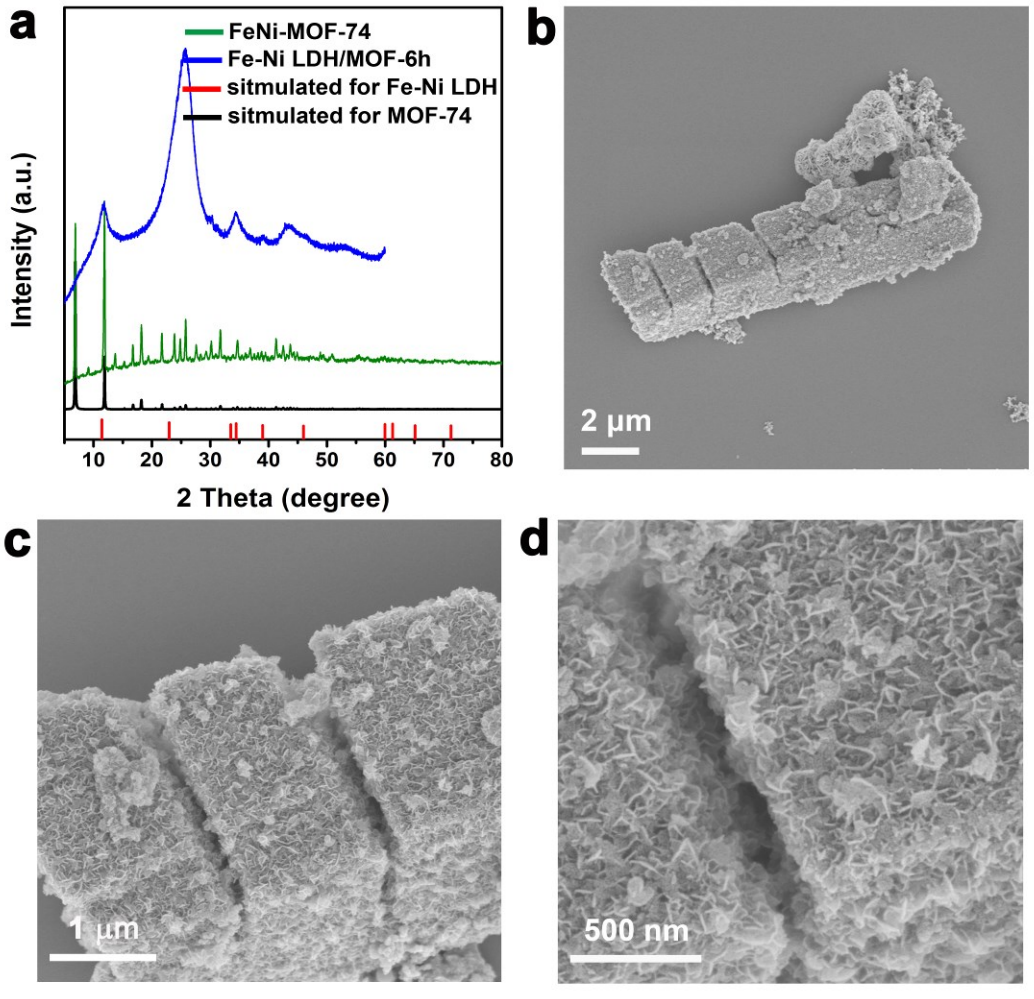


**Fig. S37** XRD and SEM images for Fe-Ni LDH/MOF-b2 after 24 h stability test.

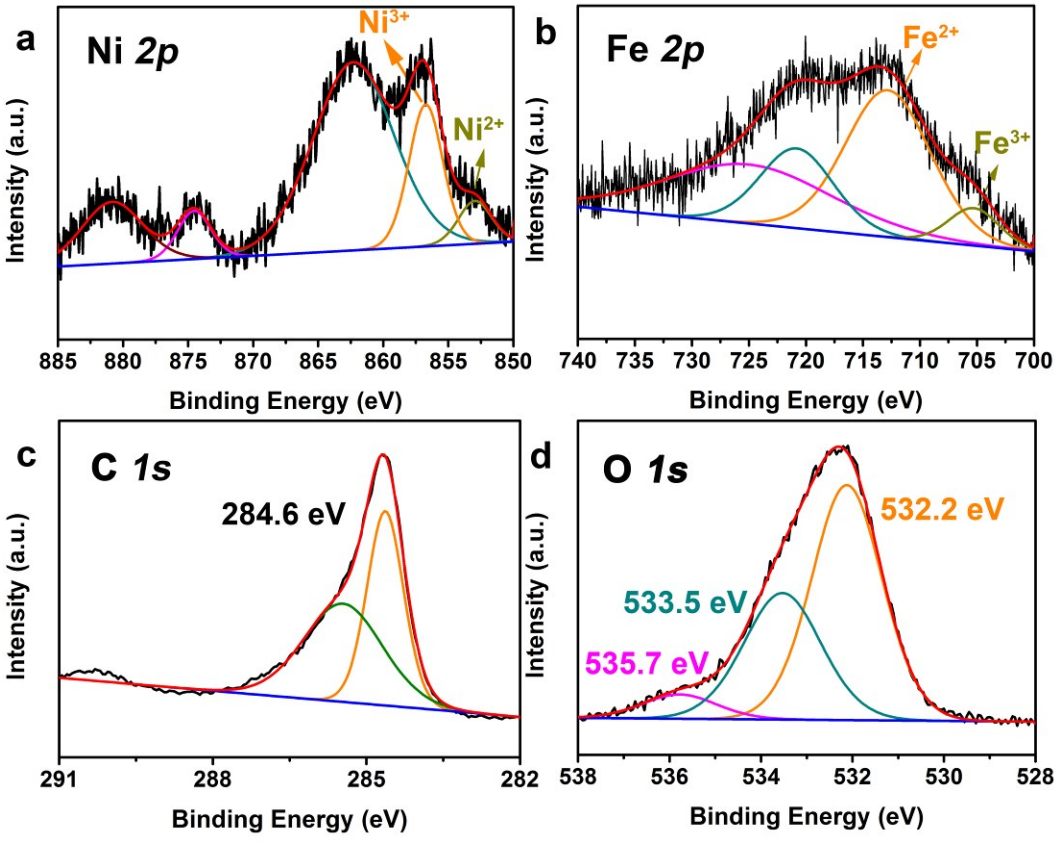


**Fig. S38** High-resolution XPS spectra of Ni *2p*, Fe *2p*, C *1s* and O *1s* for Fe-Ni LDH/MOF-b2 after 24 h stability test.